

# Pattern Formation from Defect Chaos — A Theory of Chevrons

A. G. Rossberg and L. Kramer

*Physikalisches Institut der Universität Bayreuth, D-95440 Bayreuth, Germany*

*(submitted to Physica D 23 December 1996)*

---

## Abstract

For over 25 years it is known that the roll structure of electroconvection (EC) in the dielectric regime in planarly aligned nematic liquid crystals has, after a transition to defect chaos, the tendency to form chevron structures. We show, with the help of a coarse-grained model, that this effect can generally be expected for systems with spontaneously broken isotropy, that is lifted by a small external perturbation. The linearized model as well as a nonlinear extension are compared to simulations of a system of coupled amplitude equations which generate chevrons out of defect chaos. The mechanism of chevron formation is similar to the development of Turing patterns in reaction diffusion systems.

---

## 1 Introduction

Understanding defect chaotic states of pattern forming systems is presently one of the important goals of research in pattern formation [1]. Important questions relate to the physical quantities characterizing properly such a state [2–6] and to the possibility to observe and understand transitions between different types of defect chaos [4,7].

An interesting candidate for such a transition is the formation of chevron patterns occurring in particular in the dielectric regime of electroconvection (EC) in thin layers of planarly aligned nematic liquid crystals [8–11,13]. Increasing the ac voltage applied across the layer (above the "cutoff frequency") one first observes a (nearly) periodic pattern of (narrow) convection rolls with wavevector parallel to the director orientation imposed by surface treatment of the plates forming the upper and lower boundaries of the layer. Then defects (dislocations) in the roll pattern start to appear, their density increasing as the voltage rises. Initially they move irregularly and their distribution is homogeneous. Defects carry a topological charge which is +1 or –1 depending

on whether a roll “ends” or “begins” at that point. After a further increase of the voltage one observes the transition to chevron patterns, with defects of equal charge ordering along periodically arranged domains oriented parallel to the original roll direction. Simultaneously with the onset of the ordering process the increase of the number of defects with voltage becomes noticeably steeper [14]. Between the chains the convection rolls are rotated away from their original direction alternatingly to the left and to the right, which gives the whole structure a “herringbone” like appearance.

In this work it will be argued, that the tendency of a 2-d anisotropic pattern-forming system to form chevron patterns is a rather general feature depending in particular on symmetry properties. As a matter of fact chevron patterns as shown in Fig. 2 (for details see Sec. 5) can easily be observed in simulations of the recently proposed generic amplitude equations (1,2) [15]. This description was inspired by EC in the low-frequency conductive regime in homeotropically aligned nematics with negative dielectric anisotropy where one starts from a situation without external anisotropy (director in the  $z$  direction perpendicular to the slab). Increasing the voltage one first has a spatially homogeneous Freédericksz transition where the director bends away from the  $z$  direction thereby singling out spontaneously a direction  $\hat{c}$  in the  $x$ - $y$  plane. The isotropy may also be broken externally by applying a weak magnetic field parallel to the plain.  $\hat{c}$  may then be expressed by the angle  $\varphi$  that is enclosed by  $\hat{c}$  and the field. At higher voltages there is an instability to EC with a critical mode corresponding to rolls with wavevector parallel to the in-plane director  $\hat{c}$  (in the simplest case). A weakly nonlinear description then has to incorporate the roll mode as well as the undamped mode corresponding to (infinitesimal) rotations of  $\hat{c}$  (the Goldstone mode). Equations (1,2) below describe such a situation. In fact chevrons have recently been observed in homeotropic EC [16]. Other systems where chevrons were observed are dielectric EC under oblique boundary conditions [17], EC in nematic polymers [18] and sometimes also in the conductive regime of EC in planarly aligned ordinary nematics [19].

After introducing our notation and definitions in Sec. 2 we develop a linear and (weakly) nonlinear model of chevron structures in Secs. 3 and 4. In Sec. 5 some predictions of the model are tested quantitatively against numerical simulations of Eqs.(1,2). Section 6 discusses experimental and theoretical questions in a more general framework.

## 2 Formal Setting

The derivation from symmetry arguments of the coupled amplitude equations for systems with spontaneously (and almost spontaneously) broken isotropy is presented in [15]. (There the coefficients are also calculated from hydrodynam-

ics for EC in homeotropically oriented nematics.) The system should bifurcate supercritically to a roll pattern with wavevector parallel to  $\hat{c} = (\cos \varphi, \sin \varphi)$  (normal rolls) when some external control parameter  $\varepsilon$  changes sign from negative to positive. For small  $\varepsilon$  and  $\varphi$  and after some rescaling the equations take the form

$$\tau \partial_t A = (1 + \partial_x^2 + (\partial_y - i\varphi)^2 + i\beta_y \varphi_{,y} - |A|^2) A, \quad (1)$$

$$\begin{aligned} \partial_t \varphi &= (K_3 \partial_x^2 + \partial_y^2 - H^2/\varepsilon) \varphi + \\ &\Gamma(-iA^*(\partial_y - i\varphi)A + c.c.). \end{aligned} \quad (2)$$

In Eq.(1) the derivative operator  $\partial_y$  operates only on  $A$  and  $\varphi_{,y} := \partial\varphi/\partial y$ . All coefficients are real,  $\tau$  and  $K_3$  are positive.  $A$  is the complex amplitude of the patterning mode.  $A = \text{const.}$  corresponds to the most unstable linear mode at  $\varphi = 0$ . Similar to the usual real Ginzburg-Landau equation a factor  $\sim \varepsilon^{-1/2}$  has been taken out of the physical length scales, a factor  $\sim \varepsilon^{-1}$  out of time, and a factor  $\sim \varepsilon^{1/2}$  out of  $A$  and  $\varphi$ . The spatial extensions of the plane  $L_x, L_y$  should be large ( $L_x, L_y \gg 1$ ). Whenever needed we will impose the convenient periodic boundary conditions. The coefficient containing  $H^2$  describes the (small) external perturbation of isotropy. (We use this notation since  $H$  is typically a (scaled) magnetic field.) For sufficiently large  $H^2$  (or, equivalently, small  $\varepsilon$  while  $H \neq 0$ ) one has a stable band of stationary, spatially periodic solutions of (1,2). All such solutions are unstable for  $H^2 = 0$  if  $\Gamma$  is negative, which appears to be typical for nematics. In simulations one typically observes a transition to a defect chaotic state when  $h^2 := H^2/(-2\Gamma\varepsilon)$  drops below a critical value of  $O(1)$  [15].

Writing the complex amplitude  $A$  as  $A = |A| e^{i\theta}$  defines the phase modulations  $\theta$  of the underlying stripe pattern up to multiples of  $2\pi$ . This degeneracy plays no roll as long as only

$$\nabla\theta = \text{Im} \left\{ \frac{\nabla A}{A} \right\} \quad (3)$$

is considered (and  $A \neq 0$ ).  $\nabla\theta$  is the deviation of the local wavevector from the most unstable wavevector at  $\varphi = 0$  (up to the rescaling done in Eq. (1)). The wavevector of the roll pattern and the director  $\hat{c}$  are parallel if  $P := \partial_y\theta = \varphi$ .

A topological defect in the stripe pattern corresponds to a simple zero of the complex amplitude  $A$ . Its topological charge is  $\int d\vec{r} \cdot \nabla\theta/2\pi$ , where the path of integration is a small loop encircling the defect in the positive sense.

We define defect densities

$$n_{\pm}(\vec{r}) = \sum_j \delta(\vec{r} - \vec{r}_{\pm,j}), \quad (4)$$

where the sum is over all positively or negatively charged defects at the positions  $\vec{r}_{\pm,j}$ , respectively, and  $\delta(\cdot)$  is the Dirac  $\delta$  function. The total defect density is  $n := n_+ + n_-$  and the topological charge density is  $\rho := n_+ - n_-$ . One has

$$\int_{\partial\Omega} \nabla\theta(\vec{r}) d\vec{r} = 2\pi \int_{\Omega} \rho(\vec{r}) d\Omega \quad (5)$$

for any area  $\Omega$ .

From an abstract point of view one can define chevrons as a periodic modulation of  $\rho$ , with a wavevector parallel to the  $x$  axis [11]. Hence we will only look at modulations of the defect chaotic state in the  $x$  direction and average all equations along  $y$ , which will be indicated by an overbar  $\bar{\cdot} := L_y^{-1} \int \cdot dy$ . In particular one finds a topological condition

$$\partial_x \bar{P} = 2\pi \bar{\rho}, \quad (6)$$

by differentiating both sides of Eq. (5) for a rectangular area  $\Omega = (0..\xi) \times (0..L_y)$  with respect to  $\xi$ . Obviously  $\bar{P}$  can only change through defect motion. In fact, for fixed and (locally) constant  $\varphi$ , where Eq. (1) reduces to the simple Ginzburg-Landau equation, defects always move such that the (local) wavenumber approaches the value of highest growth rate [21], which includes the condition  $P = \varphi$ .

### 3 Linear Model

A simple model for the coarse-grained dynamics of the defect-chaotic state helps to understand chevron formation as a linear modulation instability of homogeneous defect chaos. Led by symmetry considerations [15] we propose a model equation for the conservation of topological charge

$$\partial_t \bar{\rho} + \partial_x \left[ -D \partial_x \bar{\rho} + \sigma (\bar{P} - \bar{\varphi}) \right] = 0. \quad (7)$$

The diffusion coefficient  $D$  and the ‘‘conductivity’’  $\sigma$  are phenomenological constants. We do not calculate them here and assume both to be positive. This means that diffusion of defects acts to minimize topological charge imbalance and systematic drift acts to reduce  $|\bar{P} - \bar{\varphi}|$ . To get a corresponding equation for  $\varphi$  we average Eq. (2) over  $y$ .

$$\partial_t \bar{\varphi} = (K_3 \partial_x^2 + 2\Gamma h^2) \bar{\varphi} + 2\Gamma |A|_{\text{eff}}^2 (\bar{P} - \bar{\varphi}). \quad (8)$$

The form of the last term follows from isotropy for small  $\bar{P} - \bar{\varphi}$ ,  $|A|_{\text{eff}}^2$  is a suitable constant. Equations (6,7,8) describe dynamics for small deviations from  $\bar{p} = 0$  on scales much larger than  $n^{-1/2}$ .

Using this model one can calculate the stability of homogeneous defect-chaotic solutions against periodic modulations of  $\bar{P}$  and  $\bar{\varphi}$  in  $x$  direction. After applying  $\partial_x$  on Eq. (8) and eliminating  $\bar{P}$  through (6), Eqs. (7,8) take the form of a linearized reaction diffusion system for  $\bar{p}$  and  $\partial_x \bar{\varphi}$ . Accordingly one gets a homogeneous Hopf bifurcation or a steady state, spatially periodic (diffusive) Turing instability or a simple non oscillatory, homogeneous bifurcation as the first instability (see e.g. [22,23]).

For  $K_3/D > 1$  and  $1 < -\Gamma|A|_{\text{eff}}^2/\pi\sigma$ , or  $K_3/D < 1$  and  $(D/K_3)^{1/2} + (K_3/D)^{1/2} < 2(-\Gamma|A|_{\text{eff}}^2/\pi\sigma)^{1/2}$  one has the Hopf bifurcation at  $h_{\text{Hopf}}^2 = |A|_{\text{eff}}^2 + \pi\sigma/\Gamma$ . The Hopf frequency is  $\omega_{\text{Hopf}}^2 = 4\pi\sigma(-\Gamma|A|_{\text{eff}}^2 - \pi\sigma)$ .

If  $(D/K_3)^{1/2} + (K_3/D)^{1/2} > 2(-\Gamma|A|_{\text{eff}}^2/\pi\sigma)^{1/2}$  and  $K_3/D < -\Gamma|A|_{\text{eff}}^2/\pi\sigma$  the chevron (“Turing”) pattern with critical wavenumber  $k_c^2 = (-4\pi\Gamma|A|_{\text{eff}}^2\sigma/DK_3)^{1/2} - 2\pi\sigma/D$  appears first at  $h_c^2 = (|A|_{\text{eff}} - (\pi K_3\sigma)^{1/2}(-D\Gamma)^{-1/2})^2$  (see also Fig. 1).

None of the two instabilities occurs in the remaining case that  $K_3/D > -\Gamma|A|_{\text{eff}}^2/\pi\sigma$  and  $1 > -\Gamma|A|_{\text{eff}}^2/\pi\sigma$ . At  $h^2 = 0$  the mode of homogeneous rotation (Goldstone mode) invokes instability.

According to this model a crucial effect is the diffusive contribution in Eq. (7). It invokes a wavevector mismatch ( $P - \varphi$ ) for modulated  $P$  and  $\varphi$  which would otherwise be leveled out by defect motion. Due to this mismatch the repulsive “torque” on  $\varphi$  by the roll pattern (described by the term containing  $\Gamma$  in Eq. (8)) can then drive chevron formation. It should be noted that no particular assumption about the interaction of single defects was made. By inspection one finds that the model is robust against additional terms in Eq. (7), as long as modulations of  $P$  are weakened compared to modulations of  $\varphi$ . For example, a consistent truncation in powers of  $k$  should include a fourth-order diffusive term in Eq. (7) that has been avoided for the sake of simplicity.

## 4 Nonlinear Model

In the final, saturated chevron pattern the defect density  $n$  becomes strongly modulated with half the period of the chevron pattern. The defects accumulate along “chains”. This can be understood with ideas similar to those describing a p-n junction in a semiconductor. In the regions along the chains a high density of positively or negatively charged defects is enforced by the strong bent ( $\partial_x \varphi$ ) of the director. This corresponds to doping the p and n regions of

the semiconductor with charge carriers. The density of the oppositely charged species is strongly suppressed due to high recombination probability. As in the depletion layer of the p-n junction, in the region between the chains the *total* density of defects  $n$  is reduced compared to the “chain” region.

The coupling between  $\rho$  and  $n$  may also provide an important contribution to the nonlinear saturation of the chevron mode. Assume that defects are homogeneously created at a constant rate  $n_0/\tau_n$ , while they are annihilated at a rate proportional to  $n_+n_-$ , such that for the homogeneous defect chaos one has a time-averaged defect density  $\langle n \rangle_t = 2n_0$  (In this section we only consider quantities averaged over  $y$  and drop the overbars.) Ignoring correlations in the nonlinear terms we obtain

$$\partial_x j_{\pm} + \partial_t n_{\pm} = \frac{1}{\tau_n n_0} (n_0^2 - n_+ n_-), \quad (9)$$

where  $j_{\pm}$  are the defect currents. Since  $n_0^2 - n_+ n_- = n_0^2 - n^2/4 + \rho^2/4$  an excitation of the chevron mode increases the equilibrium number of defects. One should expect that with increased defect density  $n$  the conductivity  $\sigma$  becomes higher (e.g.  $\sigma = mn$  with some mobility constant  $m$ ). This weakens the relative importance of the diffusive term in Eq. (7) so that the chevron mode saturates. In order to get a quantitative estimate of this effect we calculated the weakly nonlinear [20] steady state solution of Eqs. (8,9), assuming currents of the form

$$j_{\pm} = -D\partial_x n_{\pm} \pm m n_{\pm} (P - \varphi), \quad (10)$$

and allowing for a modulated value of  $|A|_{\text{eff}}^2$  by substituting

$$|A|_{\text{eff}}^2 \rightarrow |A|_{\text{eff}}^2 (1 - c_1 n - c_2 \rho^2 - c_3 (P - \varphi)^2) \quad (11)$$

in Eq. (8).

For periodic solutions with wavevector  $k$  one obtains, up to a phaseshift,

$$P = \sqrt{\frac{(h_c^2 - h^2)}{G}} \sin kx + O(h_c^2 - h^2)^{3/2}, \quad (12)$$

$$\varphi = \left(1 + \frac{Dk^2}{4\pi n_0 m}\right) P + O(h_c^2 - h^2)^{3/2}, \quad (13)$$

$$n = 2n_0 + \frac{k^2 (h_c^2 - h^2)}{16\pi^2 n_0 G} \cos^2 kx + O(h_c^2 - h^2)^2, \quad (14)$$

with

$$\begin{aligned}
G = & -Dk^4 |A|_{\text{eff}}^2 (64\pi^2 m^2 n_0^2 (Dk^2 + 4\pi m n_0)^2)^{-1} \times \\
& [2\pi m^3 n_0 + \\
& c_1 (Dk^2 m^2 n_0 + 4\pi m^3 n_0^2) + \\
& c_2 (4Dk^2 m^2 n_0^2 + 16\pi m^3 n_0^3) + \\
& c_3 (12\pi D^2 k^2 m n_0 + 3D^3 k^4) ].
\end{aligned} \tag{15}$$

Here  $h_c^2 = h_c^2(k)$  is the value of  $h^2$  where modulations with wavevector  $k$  become unstable.

Note the following points: The result is independent of  $\tau_n$ . However, this degeneracy can be removed, e.g. by introducing cross diffusion terms  $-D_2 \partial_x n_{\mp}$  in Eq. (10). Another consequence of the particular form of Eqs. (9,10) is the simple relation

$$\tilde{n}_{2k,0} = \frac{|\tilde{\rho}_{k,0}|^2}{4n_0} \tag{16}$$

between the Fourier modes of  $\rho$  and  $n$  [we define the Fourier transform  $\tilde{f}$  of a function  $f$  by  $f(x, y) = \sum_{k,l} \tilde{f}_{k,l} \exp i(kx + ly)$ ]. To lowest order one has  $n - 2n_0 \sim \cos^2 kx$ , so that right between the chains there is no net effect of the pattern on the value of  $n$ . Both results should allow a simple comparison with experimental chevrons.

## 5 Comparison with Simulations

As pointed out in the introduction, chevron patterns are easily generated by simulating our “microscopic equations” (1,2). Figures 2 and 7 show snapshots of the steady state for different sets of parameters.

For the semi-quantitative test of our model we used a pseudo-spectral algorithm on a  $128 \times 128$  grid with spatial extensions  $L_x = 159.63$ ,  $L_y = 60.125$  and periodic boundary conditions.

The set of parameters in (1,2) was chosen in such a way that the chevron bifurcation sets in with a small wavevector. Moreover we made sure, that the oscillatory mode is absent. These conditions are satisfied by keeping

$$\begin{aligned}
\tau = 1.53558, \quad \beta_y = 1.07013, \\
K_3 = 0.180594, \quad \Gamma = -0.0304092
\end{aligned} \tag{17}$$

fixed, while taking  $h^2$  as a control parameter. We remind that the chevron

amplitude increases by *lowering*  $h^2$ . The condition of small  $k_c$  implies also  $h_c^2(k_c)$  to be small and consequently the supercritical range is rather small, too.

The most basic assumption of the model is that, to linear order, the dynamics of  $\bar{P}$  and  $\bar{\varphi}$  may be isolated from the remaining degrees of freedom and can be described by a set of linear PDEs, even though the full dynamics of  $A$  is strongly nonlinear. The coupling to the other degrees of freedom should be describable by adding noise. Close to the chevron instability, where one of the branches of eigenvectors of these linear PDEs is strongly excited by the noise, there should be a strong correlation between the Fourier modes of  $P$  and  $\varphi$ . Figure 3 shows the correlation coefficient  $r(k) = \text{Re}\langle\tilde{P}_{k,0}\tilde{\varphi}_{k,0}^*\rangle_t/(\langle|\tilde{P}_{k,0}|^2\rangle_t\langle|\tilde{\varphi}_{k,0}|^2\rangle_t)^{1/2}$  for  $h^2 = 0.025$ . Clearly there is essentially perfect correlation for  $k < 0.24$ . The sharp drop of  $r(k)$  at  $k \approx 0.3$  may be partly due to a change of the relative sign of  $P_{k,0}$  and  $\varphi_{k,0}$  in the linear mode.

In order to test the usefulness of the particular form (7,8) of the PDEs we first developed methods to “measure”  $\sigma$  and  $D$  in simulations. To find  $\sigma$ , the Fourier mode  $\tilde{\varphi}_{0,0}$  of  $\varphi$  is fixed at some finite value  $\varphi_0$ , while all other modes evolve according to Eq. (2). This was implemented by resetting  $\tilde{\varphi}_{0,0}$  to  $\varphi_0$  after each time step. The simulation is run until a steady state is reached. Then  $\varphi_0$  is set equal to zero. The relaxation rate of the global average of  $P$  equals  $2\pi\sigma$ . Figure 4 shows the average value of  $P$  as a function of the time  $\Delta t$  after switching  $\varphi_0$  to 0. Within the accuracy obtained, the decay is exponential.

Similarly, in order to measure  $D$ , a single pair of long wavelength Fourier modes  $\tilde{\varphi}_{k_0,0}$ ,  $\tilde{\varphi}_{-k_0,0}$  of  $\varphi$  was held fixed at a finite value  $\varphi_0$ .  $D/\sigma$  can be calculated from the steady state average value of  $\tilde{P}_{k_0,0}$  by setting  $\partial_t\bar{\rho} = 0$  in Eq. (7). The values for  $\sigma$  and  $D$  obtained for different values of  $\varphi_0$  and  $k_0$  were consistent. As a simple estimate for  $|A|_{\text{eff}}^2$  and  $n_0$  we took the spatial and temporal average of  $|A|^2$  and  $n/2$ .

The numerically calculated coefficients at  $h^2 = 0.025$  are

$$\begin{aligned} |A|_{\text{eff}}^2 &= 0.7996(4), & n_0 &= 0.00509(10), \\ D/\sigma &= 38.0(1.3), & \sigma &= 0.01330(73). \end{aligned} \tag{18}$$

Error estimates contain only stochastic contributions. From the linear model one then calculates the threshold  $h_c^2 = 0.037(5)$  and the critical wavenumber  $k_c = 0.214(5)$ .

Critical slowing down and strong noise make a precise determination of the threshold in simulations difficult. Since we expect  $h_c^2$  to be close to zero, where



the Goldstone mode becomes unstable, the straight forward method of extrapolating the supercritical modulation amplitude to zero cannot be applied. Instead we looked at the subcritical excitation of linear modes by noise. Without nonlinear interaction one expects a relation of the type  $\langle |\tilde{\rho}_{k,0}|^2 \rangle_t^{-1} \sim -s_k(h^2)$ , where  $s_k(h^2)$  is the growth rate of the linear mode at wavevector  $k$ . Figure 5 shows some numerical results for  $\langle |\tilde{\rho}_{k,0}|^2 \rangle_t^{-1}$  at various values of  $k$ . The dotted line is a linear fit to  $k = 0.19680$ , which implies a threshold value of  $h_{c,\text{num}}^2 \approx 0.01$ . At  $h_{c,\text{num}}^2$ , however, the  $k = 0.19680$  mode itself is already strongly suppressed by nonlinear interaction with other modes. We believe that the discrepancy between  $h_c$  and  $h_{c,\text{num}}$  is to a large part an effect of the combination of nonlinearity and strong noise. For further discussion see next section. Figure 7 shows the fully excited chevron pattern at  $h^2 = 0.005$ .

We tested two aspects of the nonlinear model. Firstly, we find Eq. (16) to be well satisfied, as long as only one mode is active. In Fig. 6 the distribution of pairs  $(|\tilde{n}_{2k,0}|, |\tilde{\rho}_{k,0}|^2)$  and the theoretical line for  $k = 0.19680$  and  $h^2 = 0.025$  are shown. While  $|\tilde{\rho}_{k,0}|^2$  is large the other modes are suppressed nonlinearly and the single mode approximation made in Eq. (16) is legitimate whereas when  $|\tilde{\rho}_{k,0}|^2$  is small the influence of competing modes becomes noticeable.

Secondly, we tested the prediction of Eq. (12) with (15) and (6) for the chevron amplitude. Due to the intricate situation at threshold our simple result cannot give more than an order of magnitude estimate. The solid line plotted in Fig. 5, shows the prediction of formula (5). It was calculated using coefficients as for the linear model with  $k = k_c$ ,  $m = \sigma/2n_0 = 1.31(8)$  and  $c_1, c_2, c_3 = 0$  without any fitting. It is easily seen that in our case the terms containing  $c_1, c_2, c_3$  give only small corrections as long as  $c_1, c_2, c_3 = O(1)$ .

The Hopf bifurcation predicted by our model can actually be found in simulations of Eqs. (1,2). For example, at  $\tau = 2.19369$ ,  $\beta_y = 1.07013$ ,  $K_3 = 0.338614$ ,  $\Gamma = -0.0608184$  and  $h^2 = 0.1$  one gets  $|A|_{\text{eff}}^2 = 0.7409(5)$ ,  $\sigma = 0.01075(36)$  and  $D/\sigma = 44.4(2.2)$ . From this the Hopf threshold is found to be  $h_{\text{Hopf}}^2 = 0.186(19)$ . The frequency of the  $k = 0$  eigenmode is  $\omega^2 = -4\pi\Gamma|A|_{\text{eff}}^2\sigma - [\Gamma(|A|_{\text{eff}}^2 - h^2) - \pi\sigma]^2 = (0.0282(7))^2$  which is in good agreement with the maximum of the Fourier transform of the simulated time series of  $\tilde{\varphi}_{0,0}$  shown in Fig. 8.

## 6 Discussion

As mentioned in the introduction the most striking case of experimental chevron formation occurs in the dielectric regime of electroconvection in planar oriented nematics. At first glance one would not expect this system to fall into the class described by the theory, Eqs. (1,2), because here the horizon-

tal orientation of the nematic director  $\hat{n}$ , which would represent the isotropy breaking degree of freedom, is fixed by the boundaries which have been prepared to align the director in one direction. However, in the dielectric regime the wavelength of the convection pattern is essentially independent of, and usually much smaller than the thickness of the layer  $d$  [24]. Then the boundaries can be reduced to a perturbative effect that may be described by the term  $H^2\varphi$  in Eq. (2).

It is not easy to verify the validity of our model for planar dielectric EC. The most important prediction is the relation between the local wavevector and the director. A straight forward polarimetric measurement of the director making use of the birefringence of the material, however, is not possible, since the polarization axis of light passing the probe follows the director essentially adiabatically. The polarization axis is therefore determined by the boundaries. Some evidence for our model can be taken from the fact, that in the regime of strongly developed chevrons, where the local wavevector is turned by nearly  $\pi/2$ , new structures form inside the nematic, which superimpose with the chevron pattern. They allow an interpretation as disclination lines resulting from the fact that in the midplane the degenerated directions  $\hat{n}$  and  $-\hat{n}$  reconnect, which cannot occur at the boundaries [17].

Defects in experimental chevrons can align much better along chains than has been found in the simulations. This is presumably because higher-order terms and non-adiabatic effects that couple the defect cores to the underlying roll structure are not included in the amplitude equations. When experimental chevron patterns are strongly excited it is usually observed, that defects start to move along the chains, alternatingly ‘up’ and ‘down’, i.e. there is a correlation between  $\partial_x\varphi$  and the  $y$  component of the velocity of a defect (ignoring its charge). This can not be observed in simulations of Eqs. (1,2). In fact, it is forbidden by the accidental symmetry  $\varphi \rightarrow -\varphi$ ,  $A \rightarrow A^*$  of Eqs. (1,2). Inclusion of higher order terms would break this symmetry. In contrast the invariance under  $\varphi \rightarrow -\varphi$ ,  $y \rightarrow -y$ , which follows from inversion symmetry [15], remains.

We wish to emphasize that chevrons cannot appear directly from the homogeneous (basic) state via a stationary supercritical bifurcation. Although this is consistent with most experiments there is some evidence that at sufficiently high frequencies chevrons can be observed directly at onset of the dielectric instability [11]. This would mean that either the primary bifurcation becomes subcritical, which is not expected from theory, or there is a (“hidden”) bifurcation leading to an inhomogeneous state already below the dielectric instability. According to some older measurements the possibility of a first transition to a state with “wide domains” (with width  $\sim d$ ) appears to exist [25–27,18], but this phenomenon has not been cleared up. In any case this cannot be the general explanation.

It has been speculated that chevrons can be understood as a kind of interference effect between the two most unstable dielectric modes, which differ in their  $z \rightarrow -z$  symmetry. Because of the character of the dielectric rolls (wavelength much smaller than  $d$ ) the growth rates of these modes differ very little (as is the case for the higher  $z$  modes) [11]. The model has not been worked out, and can, in our view, not explain chevrons.

It might be interesting to approach the chevron transition from the point of view of phase transition theory. We are dealing with a breaking of a continuous symmetry in two dimensions of the same symmetry class as the  $x$ - $y$  model. Therefore the transition is, at least when nonadiabatic effects are neglected, possibly of the Kosterlitz-Thouless type [28]. The model given here represents a simplified, mean-field type description. Consequently it is not surprising that the transition is delayed and difficult to pin down in the full “microscopic” theory described by Eqs. (1,2).

Finally we wish to point out that chevron-like structures have also been found in simulations of the anisotropic version of the well-known complex Ginzburg-Landau equation [29]. The mechanism operative here is presently under investigation.

## Acknowledgement

We wish to thank W. Pesch for useful discussions and the experimental groups in Budapest (A. Buka and P. Toth), Leipzig (H. Amm and R. Stannarius) and Bayreuth (C. Haite, J. Peinke, and M. Scheuring) for sharing their results with us previous to publication. Financial support by Volkswagen Stiftung and Deutsche Forschungsgemeinschaft is gratefully acknowledged.

## References

- [1] M. C. Cross and P. C. Hohenberg, *Science* **263**, 1569 (1994).
- [2] L. Gil, J. Lega, and J. Meunier, *Phys. Rev. A* **41**, 1138 (1990).
- [3] I. Rehberg, S. Rasenat, and V. Steinberg, *Phys. Rev. Lett.* **62**, 756 (1989).
- [4] M. Hildebrand, M. Bär, and M. Eiswirth, *Phys.Rev.Lett* **75**, 1503 (1995).
- [5] W. Krigbaum and H. Lader, *Mol.Cryst.Liq.Cryst.* **62**, 87 (1980).
- [6] M. Caponeri and S. Ciliberto, *Physica D* **58**, 365 (1992).

- [7] T. Bohr, M. Jensen, G. Paladin, and A. Vulpiani, *Dynamical Systems Approach to Turbulence* (Cambridge University Press, Cambridge 1997).
- [8] G. Heilmeyer and W. Helfrich, Appl. Phys. Lett. **16**, 1955 (1970).
- [9] Orsay Liquid Crystal Group, Mol.Cryst.Liq.Cryst. **12**, 251 (1971).
- [10] E. Dubois-Violette, P. D. Gennes, and O. Parodi, J.Phys. (Paris) **32**, 305 (1971).
- [11] S. Kai and W. Zimmermann, Prog. Theor. Phys. Suppl. **99**, 458 (1989).
- [12] M. Scheuring, Diploma thesis, Universität Bayreuth, 1996.
- [13] P.G. de Gennes and J. Prost, *The Physics of Liquid Crystals* (Clarendon Press, Oxford 1993); L.M. Blinov, *Electrooptical and Magnetooptical Properties of Liquid Crystals* (John Wiley, New York 1983); S. Chandrasekhar, *Liquid Crystals* (University Press, Cambridge 1992).
- [14] M. Scheuring, diploma thesis, Universität Bayreuth, 1996.
- [15] A. G. Rossberg, A. Hertrich, L. Kramer, and W. Pesch, Phys.Rev.Lett. **17**, 4729 (1996).
- [16] P. Toth, Diploma thesis, Universität Bayreuth, 1996.
- [17] D. Igner and J. Freed, J.Chem.Phys **76**, 6095 (1982).
- [18] A. Trufanov, L. Blinov, and M. Barnik, Sov.Phys.JETP **51**, 314 (1980), original in Zh.Eksp.Teor.Fiz **78** 622 (February 1980).
- [19] K. Hirakawa and S. Kai, Mol.Cryst.Liq.Cryst. **40**, 261 (1977).
- [20] M. C. Cross and P. C. Hohenberg, Rev. Mod. Phys. **65**, 851 (1993).
- [21] E. Bodenschatz, W. Pesch, and L. Kramer, Physica D **32**, 135 (1988).
- [22] Y. Kuramoto, *Chemical Oscillations, Waves, and Turbulence* (Springer-Verlag, Heidelber, 1984).
- [23] H.Riecke and L.Kramer, J. Chem. Phys. **83**, 3941 (1985).
- [24] L. Kramer and W. Pesch, in *Pattern Formation in Liquid Crystals*, A. Buka and L. Kramer, eds., (Springer-Verlag, New York, 1996) p. 233.
- [25] R. Ribotta and G. Durand, J.Phys. (Paris) Colloque **C3**, 334 (1979).
- [26] L. Nasta, A. Lupu, and M. Giurgea, Mol.Cryst.Liq.Cryst. **71**, 65 (1981).
- [27] M. Barnik, L. Blinov, M. Grebenkin, and A. Trufanov, Mol.Cryst.Liq.Cryst **37**, 47 (1976).
- [28] J. Kosterlitz and D. Thouless, J. Phys. C **6**, 1181 (1972).
- [29] A. Weber, E. Bodenschatz, and L. Kramer, Advanced Materials **3**, 191 (1991).

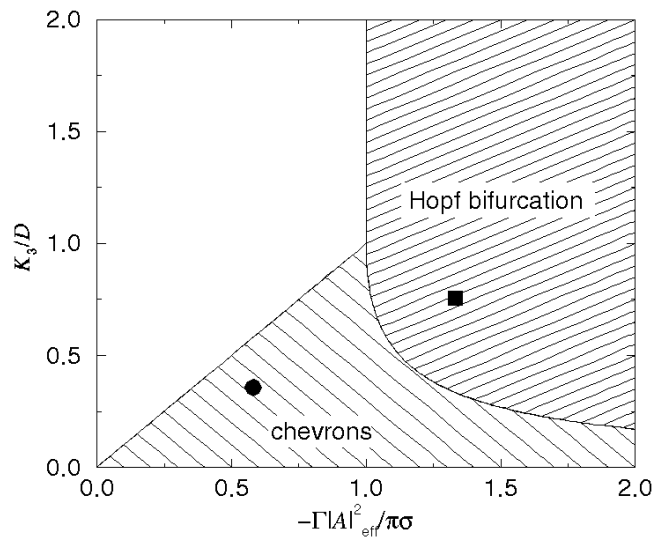


Fig. 1. Regions in parameter space where chevron instability and Hopf bifurcation respectively are the first to occur when  $h^2$  is decreased. The circle and the square correspond to the two parameter sets analyzed in Section 5.

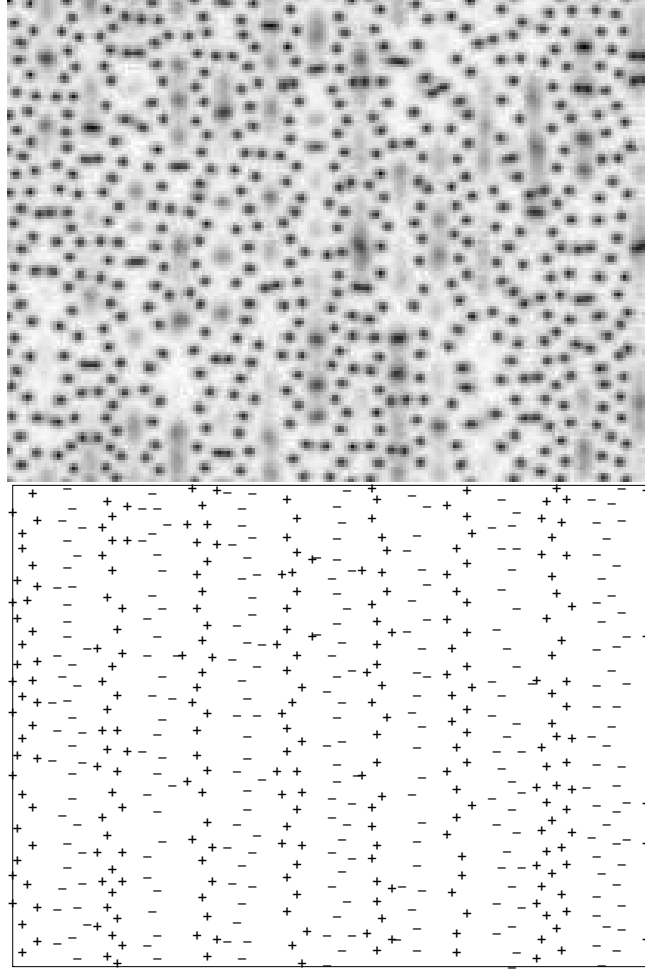


Fig. 2. Snapshot of a simulation of Eqs. (1,2) with  $\tau = 4.38738$ ,  $\beta_y = 1.07013$ ,  $K_3 = 0.0564357$ ,  $\Gamma = -0.0304092$  in a rectangle of size  $159.631 \times 120.25$ . The upper image shows  $|A|$  encoded in a grey scale, the lower one shows the positions and polarity of defects as detected by the algorithm used throughout this work.

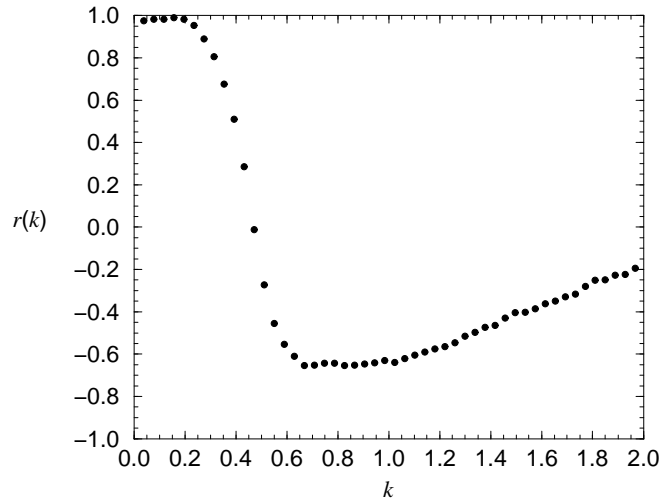


Fig. 3. Correlation between Fourier modes (see text).

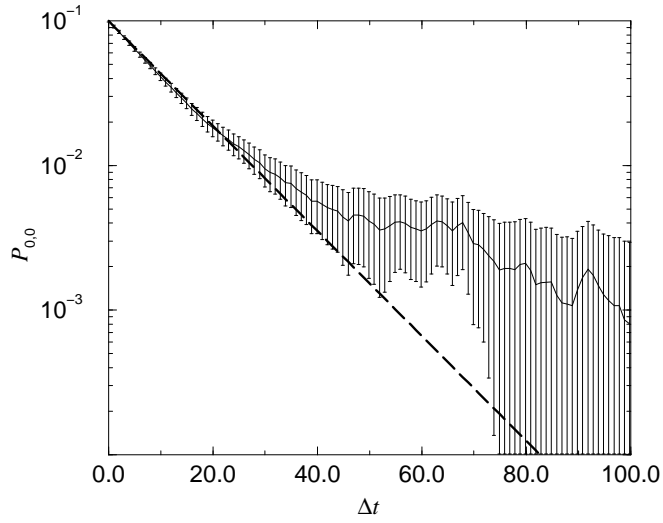


Fig. 4. Relaxation of  $\tilde{P}_{0,0}$  after a jump in  $\tilde{\varphi}_{0,0}$  from  $\varphi_0 = 0.1$  to 0, averaged over 59 runs. The dashed line is a least square fit.

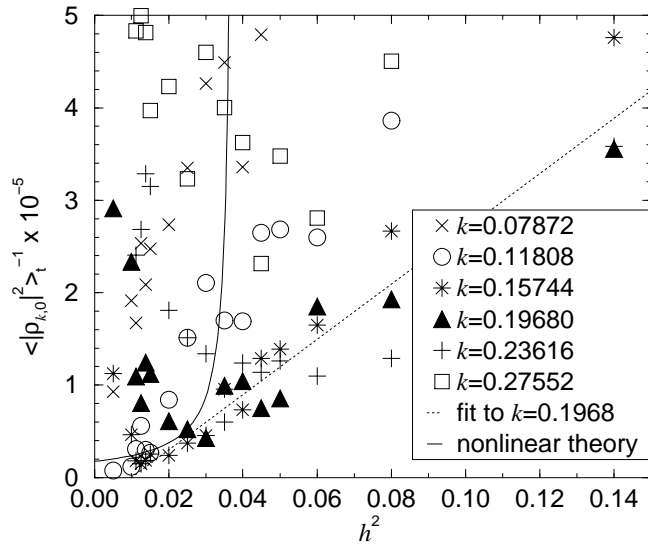


Fig. 5. Test of the linear and nonlinear model, see text.

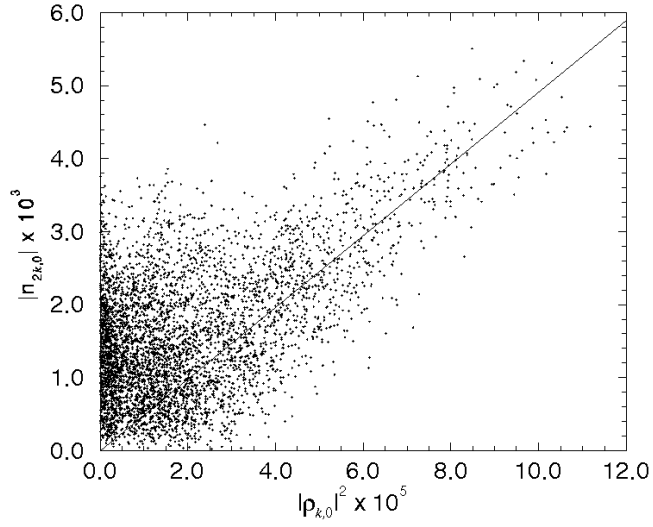


Fig. 6. Samples of pairs  $(|\tilde{n}_{2k,0}|, |\tilde{\rho}_{k,0}|^2)$  at  $k = 0.19680$  and  $h^2 = 0.025$  from numerical simulations and the relation given by (16) (solid line).

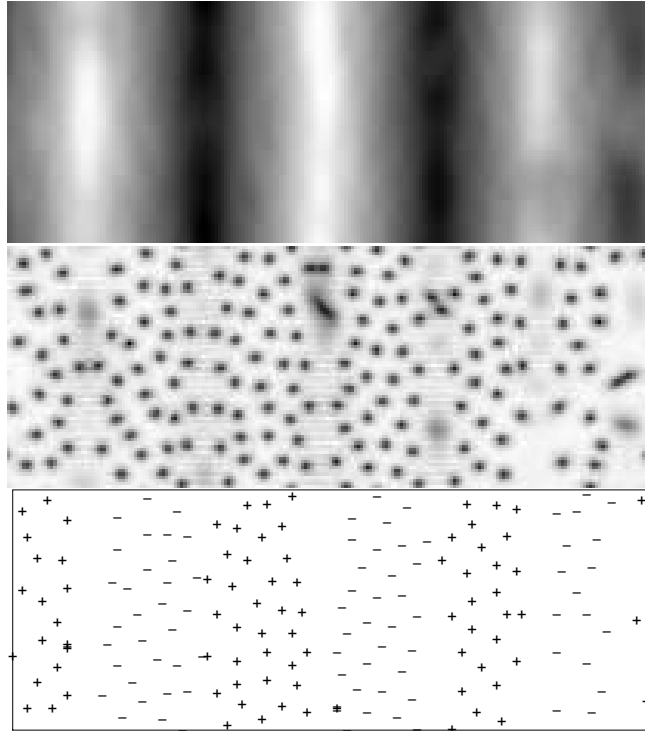


Fig. 7. Snapshot of the steady state corresponding to  $h^2 = 0.005$  in Fig. 5. Top: values of  $\varphi$  ( $-2.33 \dots 2.30$ ) encoded on a gray scale; center:  $|A|$ ; bottom: defect positions and polarities.



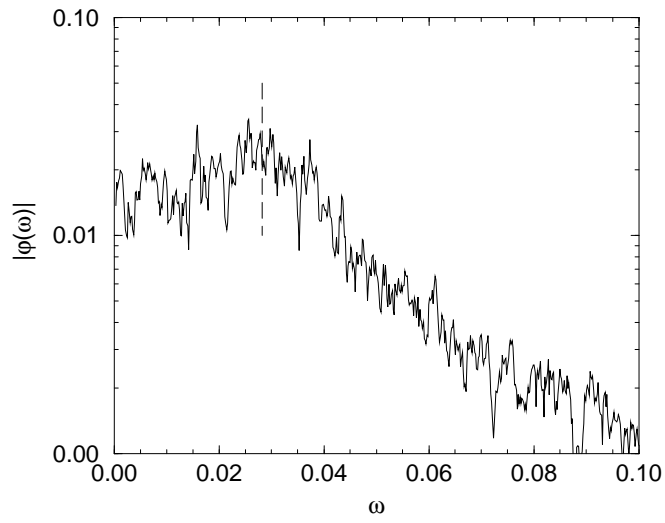


Fig. 8. Fourier transform of a simulation of Eqs. (1,2) in the oscillatory regime and the frequency of the most unstable mode of Eqs. (6–8) (dashed line). The parameters are given in the text.